Journal of Materials Chemistry A

ROYAL SOCIETY OF CHEMISTRY

PAPER

View Article Online
View Journal | View Issue

Cite this: J. Mater. Chem. A, 2025, 13, 14765

Central π-conjugated extension in quinoxaline-based small-molecule acceptors as guest components enabling high-performance ternary organic solar cells†

Chung Hang Kwok, ‡[abc] Ho Ming Ng,‡[abc] Chuanlin Gao,[d] Huawei Hu, *[e] Top Archie Dela Peña, [fg] Joshua Yuk Lin Lai,[bc] Li Chen,[bc] Lan Xie,[bc] Mingjie Li,[g] Jiaying Wu,[fh] Guangye Zhang,[d] Wai-Yeung Wong, *[ai] He Yan *[bcj] and Han Yu *[abc]

Ternary strategies have critical roles in pursuing high efficiencies for organic solar cells (OSCs). However, the optimization of ternary systems relies heavily on understanding the compatibility and performance of different guest/host combinations. To establish design principles of quinoxaline (Qx)-based small-molecule acceptors (SMAs) as guest components for ternary OSCs, a new Qx-SMA named Qx-Ac and two reported Qx-SMAs named Qx-B and Qx-Pn were synthesized by extending the central Qx core with benzene (B), acenaphthene (Ac) and phenanthrene (Pn), respectively. After blending with PM6:BTP-eC9 (17.55%), Qx-Ac (18.51%) and Qx-Pn (18.11%) devices exhibited superior phase segregation and lower energy disorder. The improvement in Qx-Pn devices was dampened by inferior absorption, while the use of Qx-B (17.56%) did not improve the device at all. This work delineates the significant influence of Qx core extension on ternary guest compatibility, providing valuable insights and guidance for the design of ternary systems towards higher efficiencies for OSCs.

Received 9th January 2025
Accepted 4th April 2025

DOI: 10.1039/d5ta00204d

rsc.li/materials-a

[a]Department of Applied Biology and Chemical Technology, The Hong Kong Polytechnic University, Hung Hom, Hong Kong, P. R. China. E-mail: wai-yeung.wong@polyu.edu.hk; yuhan.yu@polyu.edu.hk

[b]Department of Chemistry, Guangdong-Hong Kong-Macao Joint Laboratory of Optoelectronic and Magnetic Functional Materials, Energy Institute and Hong Kong Branch of Chinese National Engineering Research Center for Tissue Restoration & Reconstruction, Hong Kong University of Science and Technology, Clear Water Bay, Kowloon, Hong Kong, 999077, China. E-mail: hyan@ust.hk

[c]Guangdong-Hong Kong Joint Laboratory for Carbon Neutrality, Jiangmen Laboratory of Carbon Science and Technology, Jiangmen, Guangdong Province, 529199, China

[d]College of New Materials and New Energies, Shenzhen Technology University, Shenzhen, China

[e]State Key Laboratory for Modification of Chemical Fibers and Polymer Materials, College of Materials Science and Engineering, Donghua University, Shanghai 201620, China. E-mail: huaweihu@dhu.edu.cn

[f]Function Hub, Advanced Materials Thrust, The Hong Kong University of Science and Technology, Nansha, 511400 Guangzhou, P. R. China

[g]Department of Applied Physics, The Hong Kong Polytechnic University, Kowloon, Hong Kong, 999077, P. R. China

[h]School of Engineering, Department of Chemical Engineering, The Hong Kong University of Science and Technology, Kowloon, Hong Kong, 999077, P. R. China

[i]Research Institute for Smart Energy, The Hong Kong Polytechnic University, Hung Hom, Hong Kong, P. R. China

[j]Hong Kong University of Science and Technology-Shenzhen Research Institute, No. 9, Yuexing 1st RD, Hi-tech Park, Nanshan, Shenzhen, 518057, China

† Electronic supplementary information (ESI) available: Synthetic procedures and supplementary characterization data. See DOI: https://doi.org/10.1039/d5ta00204d

‡ These authors contributed equally.

Introduction

In recent years, organic solar cells (OSCs) have emerged as a very promising photovoltaic technology on account of their flexibility, short energy payback time and facile fabrication.[1,2] Widespread attention and extensive effort from the research community have pushed the power conversion efficiencies (PCE) of OSCs over 19% and even breaching 20% with latest development,[3–10] thanks to sophisticated molecular design of the electron acceptor.[11–17] Most of the high-achieving OSCs are constructed using the ternary strategy, which boosts device performance by broadening the active layer absorption and reducing energy loss with the inclusion of a second acceptor or donor.[18–23] The expansive array of available donors and acceptors presents a vast landscape of uncharted territory, teeming with profound insights into the design nuances of ternary guest materials which could lead to record-breaking efficiencies. To unlock this potential, it is imperative to navigate the intricate interplay between guest acceptors and host materials with precision.

The electron acceptor Y6 formed the basis of almost all high-performance acceptors today. As such, the benzothiadiazole (BT) core it uses has remained the primary research focus for the last few years, and is adopted by most state-of-the-art acceptors. Recently, attention has been diverted to acceptors

based on the quinoxaline (Qx) core.[24–35] These acceptors feature hypsochromic absorption due to upshifted energy levels and wider bandgaps, which often results in increased open-circuit voltage (V_{OC}) while potentially lowering short-circuit current (J_{SC}) as binary devices. In fact, Qx-based acceptors serve as excellent ternary guests for BT-based acceptors. They possess energy levels intermediary to BT-based acceptors and common wide bandgap donors like PM6, establishing an energy cascade that enhances charge transfer by reducing recombination loss and ultimately raising the device fill factor (FF).[25] Unlike the BT core, the Qx core allows further extension of the central conjugated ring system, which offers additional capacity for further halogenation and other molecular design strategies, including alkylation for miscibility fine-tuning,[36,37] leading to impressive performances in recently reported Qx-based acceptors.[38] In particular, the Qx-based acceptor core extension significantly affects the device performance, as proven in a number of studies on binary devices.[25,39–41] However, there is a lack of comprehensive studies on the compatibility of Qx-based acceptors as ternary guests to BT-based acceptors. Given their potential, it is important to determine which Qx-based extension platform is more suitable for a ternary guest acceptor with BT-based acceptors, thus guiding further molecular design efforts of developing more effective ternary strategies incorporating Qx- and BT-based acceptors together.

In this work, on top of reported Qx-based acceptors Qx-B and Qx-Pn, we have synthesized an additional Qx-based acceptor Qx-Ac. They feature Qx cores extended by a benzene ring (Qx-B), acenaphthene (Qx-Ac) and phenanthrene (Qx-Pn), respectively.[31,42] We then systematically investigated the effect of Qx core conjugated extension on ternary guest acceptors for ternary OSCs.[43] We chose the conventional PM6:BTP-eC9 as a host with a standard PCE of 17.55%. Among the ternary devices, PM6:BTP-eC9:Qx-Ac delivered the best performance of 18.51% with the highest V_{OC} (0.874 eV) and FF (79.35%). Morphology characterization revealed that Qx-Ac-based ternary devices offer purer domains, which led to mitigated recombination that was reflected in reduced non-radiative recombination loss, as shown in charge dynamics study and energy loss analysis. While the Qx-Pn-based ternary devices also benefitted from the same factors, they suffered from inferior absorption capability of Qx-Pn, leading to a less improved PCE of 18.11%. Meanwhile, the Qx-B incorporation proved to be ineffective as it did not sufficiently alter active layer properties with a PCE of 17.56%, identical to PM6:BTP-eC9. Therefore, the acenaphthene extension in Qx-Ac struck a balance, facilitating efficient charge transfer while maintaining sufficient exciton dissociation efficiency. Our study elucidated the benefits and shortcomings of varying core extensions in Qx-SMAs for ternary OSCs, providing valuable insights into the molecular design principles for Qx-SMAs and high-performance ternary OSCs.

Results & discussion

Fig. 1 shows the molecular structures of the ternary guest acceptors Qx-B, Qx-Pn, and Qx-Ac as well as the host acceptor BTP-eC9. Qx-B and Qx-Pn were synthesized according to the literature.[31,42] Qx-Ac was synthesized according to Scheme S1,† and its NMR and mass spectra are provided in the ESI.† The various central π-extensions cause noticeable differences in energy levels, which are determined by cyclic voltammetry (CV, Fig. 2a and S1†). As the Qx core is less electron-deficient than the benzothiadiazole core of BTP-eC9, all three acceptors exhibit elevated LUMO levels as well as slightly increased HOMO levels, resulting in enlarged bandgaps compared with BTP-eC9 (1.67 eV). This effect is more pronounced in Qx-Pn (1.78 eV) and Qx-Ac (1.76 eV) than in Qx-B (1.72 eV). Further, their energy levels are well aligned between the PM6 donor and BTP-eC9 host for them to act as energy cascade sensitizers, making them suitable ternary guest acceptors. Furthermore, energy levels and dipole moments of the SMAs are also calculated through density-functional theory (DFT) methods. The trend of theoretical energy levels agrees well with the experimental results (Fig. S2†). Meanwhile, increased dipole moments were observed in Qx-B (3.45 D), Qx-Ac (5.77 D) and Qx-Pn (4.08 D), compared with BTP-eC9 (0.01 D). This is a favorable guest attribute, as higher dipole moments lead to stronger intermolecular interactions, enabling them to facilitate molecular packing of the acceptor blend.[44,45] Accordingly, the enhancement should be the strongest in Qx-Ac blends.

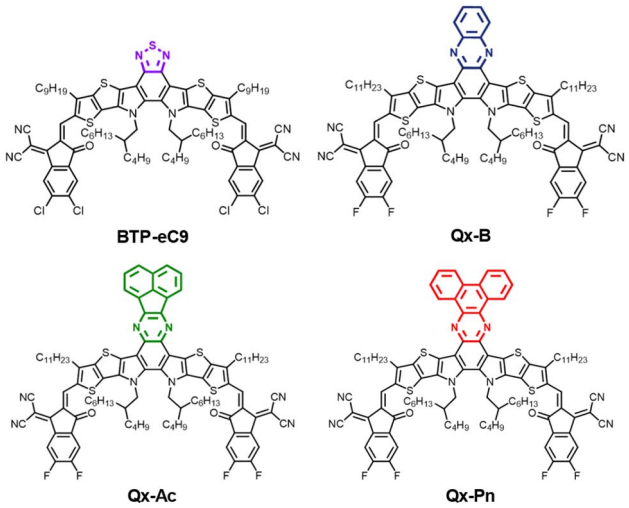

Fig. 1 Molecular structures of Qx-based guest acceptors Qx-B, Qx-Ac and Qx-Pn, as well as the BT-based host acceptor BTP-eC9.

The absorption characteristics of the materials are investigated through UV-Vis spectroscopy (Fig. 2b, c, S3 and Table S1†). The absorption maxima of Qx-B (818 nm), Qx-Ac (803 nm) and Qx-Pn (800 nm) as thin films are lower than that of BTP-eC9 (837 nm). In addition, the absorption redshift from solution to film state is also much lower in Qx-B (66 nm), Qx-Ac (54 nm) and Qx-Pn (51 nm) than in BTP-eC9 (91 nm) (Fig. S3a†). This trend is attributed to both wider bandgaps and reduced tendency of *J*-aggregation (slip-stacking) because of stronger intermolecular π–π interactions offered by the central aromatic rings, most noticeable in Qx-Pn which has the largest conjugation area and the widest bandgap.[46] With the photoluminescence spectra overlaid, conformational rigidity of the guest acceptors is also

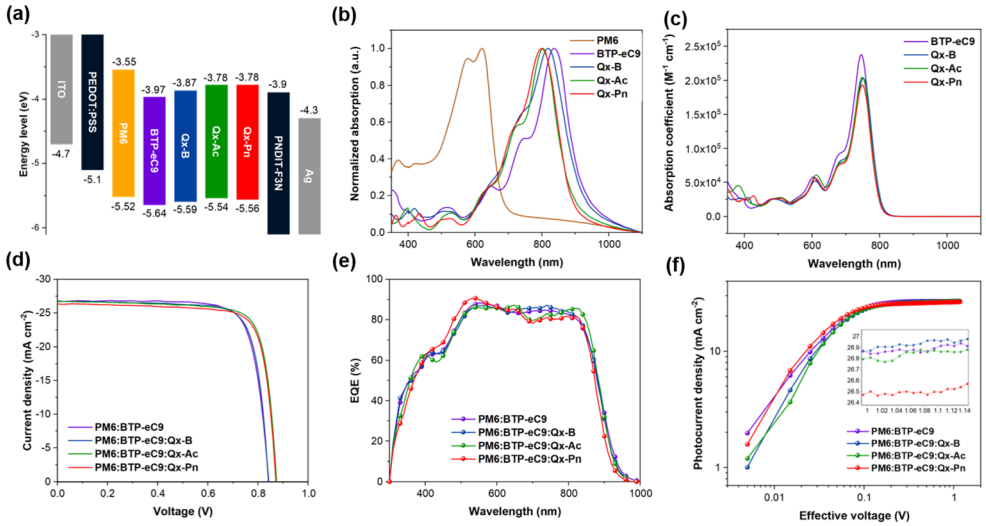

Fig. 2 (a) Energy level alignment of the device components. (b) UV-Vis absorption spectra of the PM6 donor, host and guest acceptors as thin films. (c) Absorption coefficient spectra of the acceptors in $CHCl_3$ solution. (d) Current density–voltage (J–V) curves, (e) external quantum efficiency (EQE) curves and (f) photocurrent density–effective voltage curves of the fabricated devices.

gauged *via* Stokes shift (Fig. S3b†). Qx-Ac and Qx-Pn exhibit a Stokes shift of 54 nm and 51 nm respectively, lower than 66 nm for Qx-B. This may indicate that a larger central core makes the molecule less prone to photoinduced vibrational relaxation, which mitigates nonradiative loss as revealed later. All three guest acceptors are able to provide complementary absorption with BTP-eC9, as shown by the absorption maxima at 813–819 nm for the ternary blends with PM6 and BTP-eC9 (Fig. S3c†).

To assess the performance of devices based on the Qx-based SMAs as ternary guests, ternary OSCs (and PM6:BTP-eC9 as reference) were fabricated using the conventional device structure of ITO/PEDOT:PSS/active layer/PNDIT-F3N/Ag. The detailed fabrication method could be found in the ESI.† Photovoltaic parameters of the optimized devices are listed in Table 1 (with the optimization data provided in Table S2†), and the device current density–voltage (J–V) curves are shown in Fig. 2d. PM6:BTP-eC9:Qx-B demonstrated a slightly lower V_{OC} (0.842 V) and J_{SC} (26.76 mA cm^{-2}), yet it achieves a comparable PCE of 17.56% to the host (PM6:BTP-eC9, PCE = 17.55%), thanks to a higher FF (77.93%). Both PM6:BTP-eC9:Qx-Ac and PM6:BTP-eC9:Qx-Pn record markedly improved V_{OC} (0.874, 0.872 V) and FF (79.35, 78.87%), while the Qx-Pn-based device performed worse at a relatively lower PCE of 18.11% due to the lowest J_{SC} (26.33 mA cm^{-2}) among the devices. PM6:BTP-eC9:Qx-Ac posts a less diminished J_{SC} (26.69 mA cm^{-2}) and thus outperformed other devices at a champion PCE of 18.51%. For reference, the binary Qx-based device was also fabricated with its performance listed in Table S3.† The V_{OC} and J_{SC} of the devices are consistent with the energy levels and absorption characteristics of the three Qx materials. Although these devices exhibited a significantly lower J_{SC} and FF compared with PM6:BTP-eC9, the higher V_{OC} in Qx-Ac and Qx-Pn devices explains the V_{OC} improvement when they are used as ternary guests with BTP-eC9. We also observe a lower gap in J_{SC} between Qx-Ac/Qx-Pn and Qx-B ternary devices compared with binary devices, which means that the absorption and charge dynamics must have been improved in the ternary blend.

The J_{SC}s of the devices are consistent with the calculated values from the external quantum efficiency (EQE, Fig. 2e) curves. Interestingly, the incorporation of Qx-B barely affected the photon response pattern, with PM6:BTP-eC9:Qx-B displaying similar efficiencies to PM6:BTP-eC9 across all wavelengths. In contrast, the EQE curves of the Qx-Ac and Qx-Pn ternary devices are of a different shape, where PM6:BTP-eC9:Qx-Pn excels in the 400–600 nm range whereas PM6:BTP-eC9:Qx-Ac delivers a higher response within 800–900 nm. This difference is intuitive considering the structural and energetic

Table 1 Photovoltaic parameters of the fabricated devices based on the BTP-eC9 host acceptor and Qx-B, Qx-Ac and Qx-Pn guest acceptors under the AM 1.5 G illumination of 100 mW cm^{-2}

Materials	V_{OC} (V)	J_{SC} (mA cm^{-2})	J_{cal} (mA cm^{-2})	FF (%)	PCE[a] (%)
PM6:BTP-eC9	0.843 (0.842 ± 0.001)	26.78 (26.62 ± 0.16)	26.63	77.74 (77.43 ± 0.31)	17.55 (17.38 ± 0.17)
PM6:BTP-eC9:Qx-B	0.842 (0.840 ± 0.002)	26.76 (26.61 ± 0.15)	26.60	77.93 (77.66 ± 0.27)	17.56 (17.41 ± 0.15)
PM6:BTP-eC9:Qx-Ac	0.874 (0.872 ± 0.002)	26.69 (26.57 ± 0.12)	26.56	79.35 (79.05 ± 0.30)	18.51 (18.39 ± 0.12)
PM6:BTP-eC9:Qx-Pn	0.872 (0.871 ± 0.001)	26.33 (26.19 ± 0.14)	26.21	78.87 (78.65 ± 0.22)	18.11 (17.97 ± 0.14)

[a] Average values from 16 devices shown in parentheses.

dissimilarity between Qx-Ac/Qx-Pn and BTP-eC9/Qx-B. Regardless, the Qx-Pn-based ternary device stands out performing the worst in terms of J_{SC}. Given that the absorption coefficients of Qx-based acceptors are similar (and all lower than that of BTP-eC9, Fig. 2c and S4†), the poor J_{SC} should be attributed to the absorption blueshift and charge dynamics, as evidenced later. Furthermore, saturated currents (J_{sat}) of the devices are obtained by constructing photocurrent–effective voltage curves (Fig. 2f). Given J_{max} as the current at maximum power point, the exciton dissociation probability (P_{diss}) and the charge collection probability (P_{coll}) of a device are defined as J_{SC}/J_{sat} and J_{max}/J_{sat} respectively. The ternary devices display similar P_{diss} (96.8–97.2%) and P_{coll} (90.0–91.1%) to PM6:BTP-eC9 (97.4%. 92.6%).

The surface morphology of the blend films is observed through atomic force microscopy (AFM, Fig. 3a). The surface roughness (R_q) of the ternary blend films is only a bit different than the BTP-eC9 binary blend, but it does increase with the size of central core extension, which may point to subtle variation in acceptor miscibility or solubility. Then, the molecular packing of the active layer blends is analyzed by grazing-incidence wide-angle X-ray scattering (GIWAXS, Fig. 3b, c and Table S4†).[47,48] The *d*-spacings for the low-*q* in-plane (100) lamellar stacking and high-*q* out-of-plane (010) π–π stacking are the same for ternary blends and PM6:BTP-eC9. On the other hand, the (100) and (010) coherence lengths (CCL) of the two stacking features are slightly higher in PM6:BTP-eC9:Qx-Ac (55.4, 37.7 nm) and PM6:BTP-eC9:Qx-Pn (53.3, 35.3 nm), compared to PM6:BTP-eC9 (51.4, 34.5 nm), but are lower in PM6:BTP-eC9:Qx-B (49.1, 32.3 nm). It can be drawn from the data that the Qx-Ac ternary guest enhances the molecular packing order by a small degree, while Qx-Pn and Qx-B guests exert a minimal impact on the BTP-eC9-predominated molecular packing. This trend also echoes that of the dipole moments of the acceptors, possibly indicating that the larger dipole moment in Qx-Ac contributed to the stronger

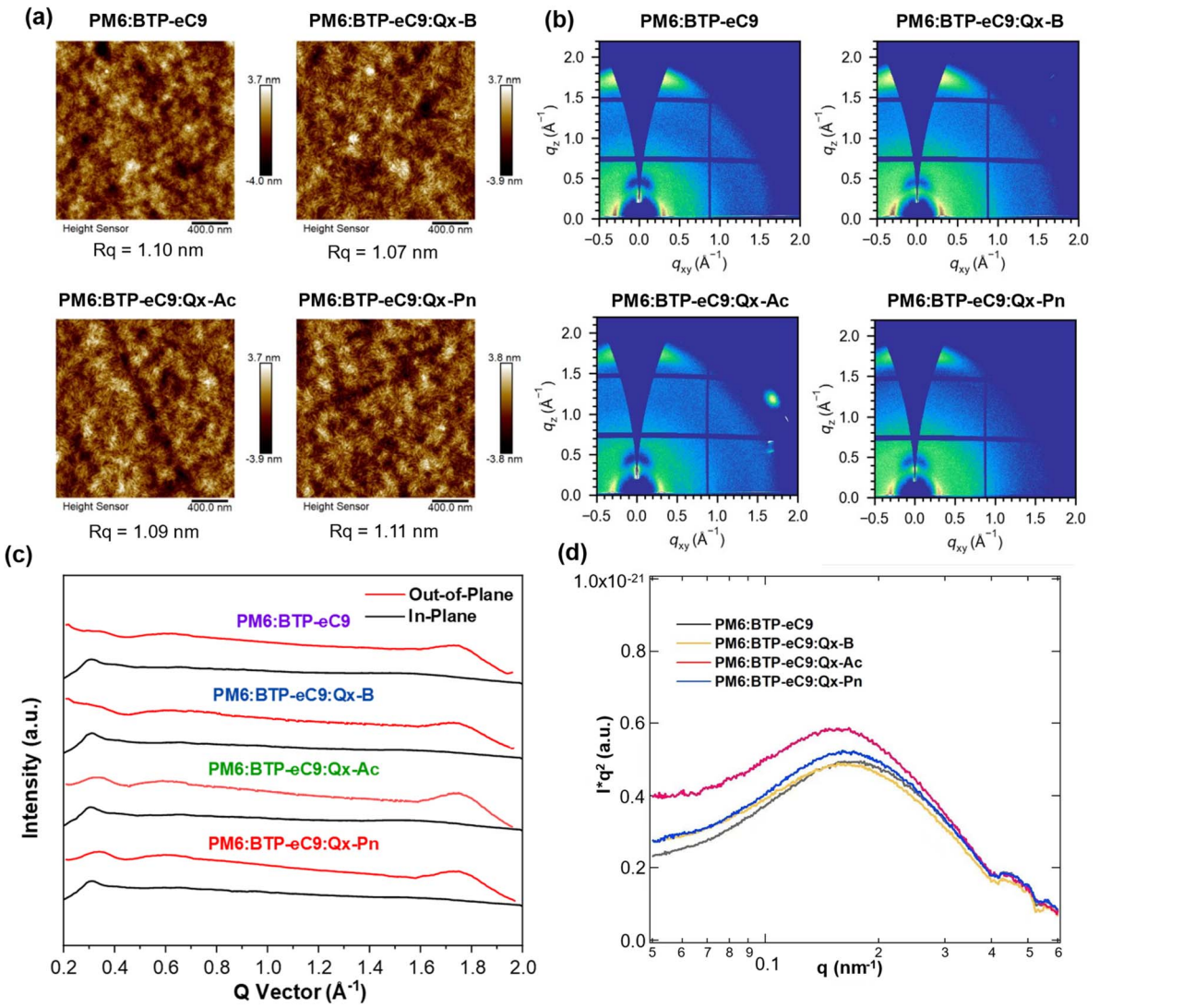

Fig. 3 (a) AFM height images and (b) 2D GIWAXS patterns of the BTP-eC9 binary and ternary blend films. (c) 1D GIWAXS line cuts of the BTP-eC9 binary and ternary blend films in the in-plane and out-of-plane directions. (d) Lorentz-corrected 1D R-SoXS profiles of the BTP-eC9 binary and ternary blend films.

molecular packing observed in its ternary blend. Subsequently, the domain features of the active layer blends are investigated through resonant soft X-ray scattering (R-SoXs, Fig. 3d).[49] While domain spacings are almost identical across the blends, the Qx-Ac and Qx-Pn ternary blends exhibit a 20% and 18% higher domain purity respectively, compared with PM6:BTP-eC9 and the Qx-B ternary blend. As revealed later, this large enhancement in domain purity contributes significantly to the higher FF observed in Qx-Ac- and Qx-Pn-based ternary devices.

Charge dynamics of the devices was investigated to rationalize the difference in device performances. Carrier sweep-out and recombination processes are evaluated by transient photocurrent (TPC, Fig. 4a) and photovoltage (TPV, Fig. 4b) separately.[50] Shorter photocurrent decay times and longer photovoltage decay times are observed in all ternary devices, with by far the most impressive improvement observed in PM6:BTP-eC9:Qx-Ac (0.169, 0.181 μs) compared to PM6:BTP-eC9 (0.221, 0.101 μs). Smaller differences are seen in PM6:BTP-eC9:Qx-Pn (0.207, 0.125 μs) and PM6:BTP-eC9:Qx-B (0.203, 0.107 μs). This implies a faster carrier sweep-out process that is less harmed by bimolecular or trap-assisted recombination loss in the ternary devices. In particular, the substantial reduction in the recombination of Qx-Ac- and Qx-Pn-based ternary devices can be attributed to their higher domain purity. These trends are well consistent with the difference in FF among the devices. However, in terms of J_{SC}, the relatively smaller enhancement in charge sweep-out and recombination loss mitigation may be insufficient in compensating for absorption blue-shift in the Qx-Pn device.

Photoluminescence (PL) quenching experiments (Fig. 4c) were conducted to gauge the charge transfer efficiencies with 514 nm (electron transfer, Fig. S5a†) and 785 nm (hole transfer, Fig. S5b†) efficiencies. The 514 nm quenching efficiency of BTP-eC9 (86.7%) is considerably worse than its 785 nm quenching efficiency (95.7%). Incorporation of ternary guest acceptors led to a great enhancement of electron transfer in Qx-Pn (89.7%), Qx-B (91.0%) and Qx-Ac (97.3%) ternary blends. On the other hand, the ternary strategy saw mixed results in hole transfer, resulting in slightly higher quenching efficiency in the Qx-Ac ternary blend (96.10%) but not in Qx-Pn (91.34%) or Qx-B (92.54%) ternary blends. Overall, PM6:BTP-eC9:Qx-Ac demonstrates a more efficient charge transfer, while PM6:BTP-eC9:Qx-B and PM6:BTP-eC9:Qx-Pn saw little overall improvement. Taking a deeper look, we further probed into the charge transfer dynamics through transient absorption spectroscopy (TAS, Fig. S6†).[51–53] The acceptor molecules were selectively excited by 800 nm pump excitation at a low fluence of 2 μJ cm^{-2}, triggering hole transfer to the donor as represented by the rise of the 560–640 nm signal band, corresponding to photobleaching (PB) by hole polaron formation (Fig. 4d). The PB rising kinetics accounts for both the exciton dissociation at the interface as well as the exciton diffusion to the interface, which are presented by the biexponential decay time constants τ_1 and τ_2 respectively.[54] The τ_1/τ_2 of PM6:BTP-eC9 is 0.86/6.24 ps. Incorporation of Qx-Pn (0.99/7.69 ps) slowed down both processes (consistent with the lowest J_{SC}), while incorporating Qx-B leads to virtually the same results (0.84/6.55 ps). In contrast, PM6:BTP-eC9:Qx-Ac demonstrates a faster τ_1/τ_2 of 0.66/5.63 ps. The difference in PB kinetics is generally consistent with the findings of the PL quenching experiment. Considering the similar P_{diss} and domain size among the devices, the PB kinetics

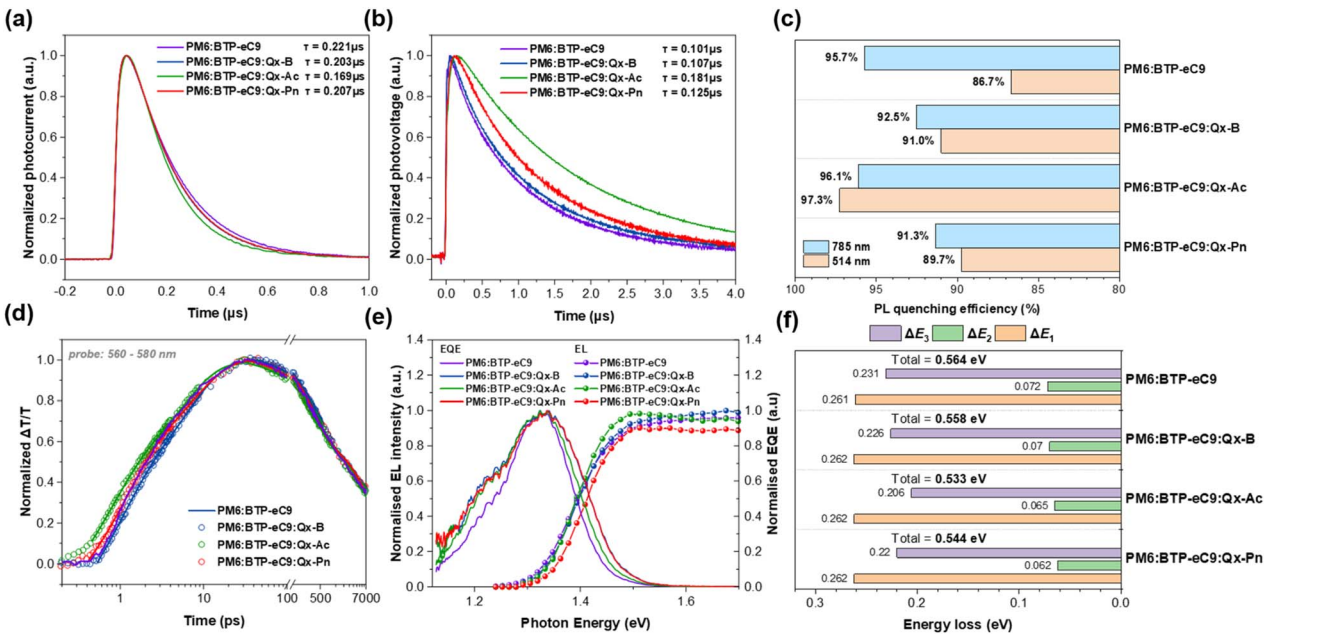

Fig. 4 (a) Transient photocurrent and (b) photovoltage decay curves of the blend films. (c) Summary of the photoluminescence quenching efficiencies of the blend films. (d) Biexponential fitting of the hole polaron photobleaching kinetics of the blend films from femto-second transient absorption spectroscopy (fs-TAS) with 800 nm pump wavelength at a fluence of 2 μJ cm^{-2}. (e) Normalized electroluminescence and EQE spectra of the devices for bandgap determination. (f) Summary of the device energy losses, including charge generation loss (ΔE_2), radiative loss (ΔE_1) and non-radiative loss (ΔE_3), with the total energy loss annotated.

can decently represent the exciton dissociation efficiencies. In particular, the higher exciton dissociation efficiency allows the Qx-Ac ternary device to overcome its inferior absorption response and generate a respectable J_{SC}, whereas the Qx-Pn ternary device fails to do so without such improvement.

Finally, energy loss (E_{loss}s) of the devices was studied by a series of photophysical experiments (Fig. 4e, f, S7 and Table S5†).[55] The intrinsic radiative recombination loss (ΔE_1) was virtually the same for all devices. Due to the reduced acceptor–donor energy offset in the guest acceptors leading to an energy cascade,[56] the loss due to charge generation ($\Delta E_2 = E_g - E_{CT}$) is reduced to 0.070, 0.065 and 0.062 eV for Qx-B-, Qx-Ac- and Qx-Pn-based ternary devices relative to the host (0.072 eV). The nonradiative recombination loss (ΔE_3) also shrank to 0.226, 0.206 and 0.220 eV for Qx-B-, Qx-Ac- and Qx-Pn-based ternary devices relative to the host (0.231 eV). This is consistent with the lessened recombination owing to purer domains in the ternary blends, as proven by TPV and R-SoXs experiments. The reduced tendency of photoinduced vibrational relaxation as evidenced by the Stokes shift may also contribute to the improvement,[57] as well as the slightly more ordered molecular packing as seen in GIWAXS. The stronger enhancement in the ΔE_3 of Qx-Ac compared with Qx-Pn is likely attributed to the slightly stronger molecular packing as evidenced by the GIWAXS results. Therefore, compared to PM6:BTP-eC9 (0.564 eV), the Qx-B-, Qx-Ac- and Qx-Pn-based ternary devices exhibit mitigated total energy loss of 0.558, 0.533 and 0.544 eV respectively, notably leading to higher V_{OC}s in the latter two devices with larger central conjugation in guest SMAs.

Conclusions

In summary, the main benefit of incorporating Qx-Ac and Qx-Pn ternary guests is establishing a more favorable domain purity, which suppresses recombination and thus realizing a smaller non-radiative loss, as reflected in higher V_{OC} and FF. The effect is more pronounced for the Qx-Ac-based device, which also demonstrates more efficient charge transfer, delivering the highest V_{OC} and FF among the devices. Meanwhile, the mixed performance of the Qx-Pn device in terms of exciton dissociation, diffusion and the overall charge dynamics means that it could not offset the higher absorption blueshift, leading to the lowest J_{SC}. Lastly, Qx-B inclusion barely affected the performance of the BTP-eC9 binary blend due to similarity to BTP-eC9 in both energetic and molecular aspects. This work has demonstrated that the acenaphthene core extension may be most desirable for a Qx-based ternary guest acceptor with a BT-based acceptor host. We recommend further investigation of possible molecular design strategies with Qx-Ac as a template, which should be focused on improving the absorption response and exciton dissociation efficiency to elevate J_{SC} of the resulting ternary device.

Data availability

The data supporting this article have been included as part of the ESI.†

Conflicts of interest

There are no conflicts to declare.

Acknowledgements

H. Yu appreciates the support from the Strategic Hiring Scheme start-up fund of the Hong Kong Polytechnic University (Project ID: P0056175; Work Programme: BDDV) and the Hong Kong Research Grants Council (GRF project 16303024 and 16310824). H. Yan appreciates the support from the National Key Research and Development Program of China (No. 2019YFA0705900) funded by MOST, the Basic and Applied Research Major Program of Guangdong Province (No. 2019B030302007), the National Natural Science Foundation of China (NSFC, No. 22075057), the Shen Zhen Technology and Innovation Commission through (Shenzhen Fundamental Research Program, JCYJ20200109140801751), the Hong Kong Research Grants Council (research fellow scheme RFS2021-6S05, RIF project R6021-18, CRF project C6023-19G, GRF project 16310019, 16310020, 16309221, 16309822), Hong Kong Innovation and Technology Commission (ITCCNERC14SC01) and Foshan-HKUST (Project No. FSUST19-CAT0202), Zhongshan Municipal Bureau of Science and Technology (No. ZSST20SC02), Guangdong-Hong Kong-Macao Joint Laboratory (No. 2023B1212120003) and Tencent Xplorer Prize. We also would like to express our gratitude to beamline BL16B1 at Shanghai Synchrotron Radiation Facility (SSRF) for their support during the GIWAXS experiment. RSoXS measurement was conducted at ALS BL 11.0.1.2, supported by the Office of Science, Office of Basic Energy Sciences, of the U.S. Department of Energy under Contract No. DE-AC02-05CH11231. W. Y. W. is grateful to the financial support from the RGC Senior Research Fellowship Scheme (SRFS2021-5S01), Research Institute for Smart Energy (CDAQ), Research Centre for Organic Electronics (CE0P), Research Centre for Carbon-Strategic Catalysis (CE2L) and Miss Clarea Au for the Endowed Professorship in Energy (847S).

Notes and references

1 G. Zhang, F. R. Lin, F. Qi, T. Heumüller, A. Distler, H.-J. Egelhaaf, N. Li, P. C. Y. Chow, C. J. Brabec, A. K.-Y. Jen and H.-L. Yip, *Chem. Rev.*, 2022, **122**, 14180–14274.

2 A. Wadsworth, M. Moser, A. Marks, M. S. Little, N. Gasparini, C. J. Brabec, D. Baran and I. McCulloch, *Chem. Soc. Rev.*, 2019, **48**, 1596–1625.

3 L. Zhu, M. Zhang, J. Xu, C. Li, J. Yan, G. Zhou, W. Zhong, T. Hao, J. Song, X. Xue, Z. Zhou, R. Zeng, H. Zhu, C.-C. Chen, R. C. I. MacKenzie, Y. Zou, J. Nelson, Y. Zhang, Y. Sun and F. Liu, *Nat. Mater.*, 2022, **21**, 656–663.

4 K. Chong, X. Xu, H. Meng, J. Xue, L. Yu, W. Ma and Q. Peng, *Adv. Mater.*, 2022, **34**, 2109516.

5 C. Guo, Y. Sun, L. Wang, C. Liu, C. Chen, J. Cheng, W. Xia, Z. Gan, J. Zhou, Z. Chen, J. Zhou, D. Liu, J. Guo, W. Li and T. Wang, *Energy Environ. Sci.*, 2024, **17**, 2492–2499.

6 J. Fu, Q. Yang, P. Huang, S. Chung, K. Cho, Z. Kan, H. Liu, X. Lu, Y. Lang, H. Lai, F. He, P. W. K. Fong, S. Lu, Y. Yang, Z. Xiao and G. Li, *Nat. Commun.*, 2024, **15**, 1830.
7 H. Yu, C. Zhao, H. Hu, S. Zhu, B. Zou, T. A. D. Peña, H. M. Ng, C. H. Kwok, J. Yi, W. Liu, M. Li, J. Wu, G. Zhang, Y. Chen and H. Yan, *Energy Environ. Sci.*, 2024, **17**, 5191–5199.
8 Z. Luo, T. Liu, R. Ma, Y. Xiao, L. Zhan, G. Zhang, H. Sun, F. Ni, G. Chai, J. Wang, C. Zhong, Y. Zou, X. Guo, X. Lu, H. Chen, H. Yan and C. Yang, *Adv. Mater.*, 2020, **32**, 2005942.
9 M. Zhang and Z.-G. Zhang, *Sci. China Mater.*, 2024, **67**, 2713–2714.
10 H. Liu, X. Gao, Y. Xin, R. Wang, H. Zhong, B. Kan, X. Wan, Y. Chen and Y. Liu, *Sci. China Mater.*, 2025, DOI: **10.1007/s40843-024-3277-8**.
11 H. Yu, M. Pan, R. Sun, I. Agunawela, J. Zhang, Y. Li, Z. Qi, H. Han, X. Zou, W. Zhou, S. Chen, J. Y. L. Lai, S. Luo, Z. Luo, D. Zhao, X. Lu, H. Ade, F. Huang, J. Min and H. Yan, *Angew. Chem., Int. Ed.*, 2021, **60**, 10137–10146.
12 H. Yu, Y. Wang, H. K. Kim, X. Wu, Y. Li, Z. Yao, M. Pan, X. Zou, J. Zhang, S. Chen, D. Zhao, F. Huang, X. Lu, Z. Zhu and H. Yan, *Adv. Mater.*, 2022, **34**, 2200361.
13 H. Yu, Y. Wang, X. Zou, H. Han, H. K. Kim, Z. Yao, Z. Wang, Y. Li, H. M. Ng, W. Zhou, J. Zhang, S. Chen, X. Lu, K. S. Wong, Z. Zhu, H. Yan and H. Hu, *Adv. Funct. Mater.*, 2023, **33**, 2300712.
14 H. Yu, Z. Qi, J. Yu, Y. Xiao, R. Sun, Z. Luo, A. M. H. Cheung, J. Zhang, H. Sun, W. Zhou, S. Chen, X. Guo, X. Lu, F. Gao, J. Min and H. Yan, *Adv. Energy Mater.*, 2021, **11**, 2003171.
15 H. Yu, S. Luo, R. Sun, I. Angunawela, Z. Qi, Z. Peng, W. Zhou, H. Han, R. Wei, M. Pan, A. M. H. Cheung, D. Zhao, J. Zhang, H. Ade, J. Min and H. Yan, *Adv. Funct. Mater.*, 2021, **31**, 2100791.
16 L. Xie, D. Qiu, X. Zeng, C. H. Kwok, Y. Wang, J. Yao, K. Ding, L. Chen, J. Yi, H. Ade, Z. Wei, W.-Y. Wong, H. Yan and H. Yu, *Sci. China Mater.*, 2025, **68**, 860–867.
17 T. Zou, Y. Gong, X. Li, G. Sun, H. M. Ng, M. Zhang, H. Yu, Z.-G. Zhang, L. Meng and Y. Li, *Sci. China Mater.*, 2025, **68**, 830–837.
18 H. Lu, W. Liu, G. Ran, J. Li, D. Li, Y. Liu, X. Xu, W. Zhang and Z. Bo, *Adv. Mater.*, 2024, **36**, 2307292.
19 J. Yi, G. Zhang, H. Yu and H. Yan, *Nat. Rev. Mater.*, 2024, **9**, 46–62.
20 Y. Wang, J. Yu, R. Zhang, J. Yuan, S. Hultmark, C. E. Johnson, N. P. Gallop, B. Siegmund, D. Qian, H. Zhang, Y. Zou, M. Kemerink, A. A. Bakulin, C. Müller, K. Vandewal, X.-K. Chen and F. Gao, *Nat. Energy*, 2023, **8**, 978–988.
21 H. Yu, Y. Wang, C. H. Kwok, R. Zhou, Z. Yao, S. Mukherjee, A. Sergeev, H. Hu, Y. Fu, H. M. Ng, L. Chen, D. Zhang, D. Zhao, Z. Zheng, X. Lu, H. Yin, K. S. Wong, H. Ade, C. Zhang, Z. Zhu and H. Yan, *Joule*, 2024, **8**, 2304–2324.
22 H. Yu, Y. Wang, X. Zou, J. Yin, X. Shi, Y. Li, H. Zhao, L. Wang, H. M. Ng, B. Zou, X. Lu, K. S. Wong, W. Ma, Z. Zhu, H. Yan and S. Chen, *Nat. Commun.*, 2023, **14**, 2323.
23 D. Sun, Z. Chen, J. Zhang, W. Song, J. Shi, J. Zhu, Y. Meng, F. Jin, S. Yang and Z. Ge, *Sci. China:Chem.*, 2024, **67**, 963–972.
24 H. Liang, X. Bi, H. Chen, T. He, Y. Lin, Y. Zhang, K. Ma, W. Feng, Z. Ma, G. Long, C. Li, B. Kan, H. Zhang, O. A. Rakitin, X. Wan, Z. Yao and Y. Chen, *Nat. Commun.*, 2023, **14**, 4707.
25 H. Liu, Z. Chen, R. Peng, Y. Qiu, J. Shi, J. Zhu, Y. Meng, Z. Tang, J. Zhang, F. Chen and Z. Ge, *Chem. Eng. J.*, 2023, **474**, 145807.
26 T. Xu, Z. Luo, R. Ma, Z. Chen, T. A. Dela Peña, H. Liu, Q. Wei, M. Li, C. Zhang, J. Wu, X. Lu, G. Li and C. Yang, *Angew. Chem., Int. Ed.*, 2023, **62**, e202304127.
27 X. Liu, Z. Zhang, C. Wang, C. Zhang, S. Liang, H. Fang, B. Wang, Z. Tang, C. Xiao and W. Li, *Angew. Chem.*, 2024, **136**, e202316039.
28 H. Chen, H. Liang, Z. Guo, Y. Zhu, Z. Zhang, Z. Li, X. Cao, H. Wang, W. Feng, Y. Zou, L. Meng, X. Xu, B. Kan, C. Li, Z. Yao, X. Wan, Z. Ma and Y. Chen, *Angew. Chem., Int. Ed.*, 2022, **61**, e202209580.
29 X. Meng, M. Li, K. Jin, L. Zhang, J. Sun, W. Zhang, C. Yi, J. Yang, F. Hao, G. Wang, Z. Xiao and L. Ding, *Angew. Chem., Int. Ed.*, 2022, **61**, e202207762.
30 D. Qiu, J. Zhang, K. Lu and Z. Wei, *Nano Res.*, 2023, **16**, 11630–11637.
31 Y. Shi, Y. Chang, K. Lu, Z. Chen, J. Zhang, Y. Yan, D. Qiu, Y. Liu, M. A. Adil, W. Ma, X. Hao, L. Zhu and Z. Wei, *Nat. Commun.*, 2022, **13**, 3256.
32 H. Chen, Z. Zhang, P. Wang, Y. Zhang, K. Ma, Y. Lin, T. Duan, T. He, Z. Ma, G. Long, C. Li, B. Kan, Z. Yao, X. Wan and Y. Chen, *Energy Environ. Sci.*, 2023, **16**, 1773–1782.
33 Y. Zou, H. Chen, X. Bi, X. Xu, H. Wang, M. Lin, Z. Ma, M. Zhang, C. Li, X. Wan, G. Long, Y. Zhaoyang and Y. Chen, *Energy Environ. Sci.*, 2022, **15**, 3519–3533.
34 Z. Zhou, W. Liu, G. Zhou, M. Zhang, D. Qian, J. Zhang, S. Chen, S. Xu, C. Yang, F. Gao, H. Zhu, F. Liu and X. Zhu, *Adv. Mater.*, 2020, **32**, 1906324.
35 Z. Yao, X. Wan, C. Li and Y. Chen, *Acc. Mater. Res.*, 2023, **4**(9), 772–785.
36 Y. Guo, Z. Chen, J. Ge, J. Zhu, J. Zhang, Y. Meng, Q. Ye, S. Wang, F. Chen, W. Ma and Z. Ge, *Adv. Funct. Mater.*, 2023, **33**, 2305611.
37 L. Chen, C. Zhao, H. Yu, A. Sergeev, L. Zhu, K. Ding, Y. Fu, H. M. Ng, C. H. Kwok, X. Zou, J. Yi, X. Lu, K. S. Wong, H. Ade, G. Zhang and H. Yan, *Adv. Energy Mater.*, 2024, 2400285.
38 Y. Lang, H. Lai, Y. Fu, R. Ma, P. W. K. Fong, H. Li, K. Liu, X. Yang, X. Lu, T. Yang, G. Li and F. He, *Adv. Mater.*, 2025, **37**, 2413270.
39 H. Lai, H. Chen, Y. Zhu, H. Wang, Y. Li and F. He, *Macromolecules*, 2022, **55**, 3353–3360.
40 X. Bi, X. Cao, T. He, H. Liang, Z. Yao, J. Yang, Y. Guo, G. Long, B. Kan, C. Li, X. Wan and Y. Chen, *Small*, 2024, 2401054.
41 F. Suárez-Blas, L. Pandolfi, M. J. Alonso-Navarro, S. Riera-Galindo, J. I. Martínez, B. Dörling, A. Funes, A. Harillo-Baños, E. Venuti, M. M. Ramos, M. Campoy-Quiles and J. L. Segura, *Adv. Energy Sustainability Res.*, 2024, **5**, 2400028.
42 H. Chen, H. Liang, Z. Guo, Y. Zhu, Z. Zhang, Z. Li, X. Cao, H. Wang, W. Feng, Y. Zou, L. Meng, X. Xu, B. Kan, C. Li, Z. Yao, X. Wan, Z. Ma and Y. Chen, *Angew. Chem., Int. Ed.*, 2022, **61**(41), e202209580.

43 Y. Cui, H. Yao, J. Zhang, K. Xian, T. Zhang, L. Hong, Y. Wang, Y. Xu, K. Ma, C. An, C. He, Z. Wei, F. Gao and J. Hou, *Adv. Mater.*, 2020, **32**, 1908205.
44 M. Li, Y. Zhou, J. Zhang, J. Song and Z. Bo, *J. Mater. Chem. A*, 2019, **7**, 8889–8896.
45 W. Gao, M. Zhang, T. Liu, R. Ming, Q. An, K. Wu, D. Xie, Z. Luo, C. Zhong, F. Liu, F. Zhang, H. Yan and C. Yang, *Adv. Mater.*, 2018, **30**, 1800052.
46 S. Ma, S. Du, G. Pan, S. Dai, B. Xu and W. Tian, *Aggregate*, 2021, **2**, e96.
47 Z. Peng, L. Ye and H. Ade, *Mater. Horiz.*, 2022, **9**, 577–606.
48 A. Mahmood and J.-L. Wang, *Sol. RRL*, 2020, **4**, 2000337.
49 X. Jiao, L. Ye and H. Ade, *Adv. Energy Mater.*, 2017, **7**, 1700084.
50 S. Wood, J. C. Blakesley and F. A. Castro, *Phys. Rev. Appl.*, 2018, **10**, 024038.
51 A. A. Bakulin, A. Rao, V. G. Pavelyev, P. H. M. van Loosdrecht, M. S. Pshenichnikov, D. Niedzialek, J. Cornil, D. Beljonne and R. H. Friend, *Science*, 2012, **335**, 1340–1344.
52 Y. Zhong, M. T. Trinh, R. Chen, G. E. Purdum, P. P. Khlyabich, M. Sezen, S. Oh, H. Zhu, B. Fowler, B. Zhang, W. Wang, C.-Y. Nam, M. Y. Sfeir, C. T. Black, M. L. Steigerwald, Y.-L. Loo, F. Ng, X.-Y. Zhu and C. Nuckolls, *Nat. Commun.*, 2015, **6**, 8242.
53 Y. Tamai, Y. Murata, S. Natsuda and Y. Sakamoto, *Adv. Energy Mater.*, 2024, **14**(7), 2301890.
54 J. Yao, T. Kirchartz, M. S. Vezie, M. A. Faist, W. Gong, Z. He, H. Wu, J. Troughton, T. Watson, D. Bryant and J. Nelson, *Phys. Rev. Appl.*, 2015, **4**, 014020.
55 T. A. Dela Peña, J. I. Khan, N. Chaturvedi, R. Ma, Z. Xing, J. Gorenflot, A. Sharma, F. L. Ng, D. Baran, H. Yan, F. Laquai and K. S. Wong, *ACS Energy Lett.*, 2021, **6**, 3408–3416.
56 S. M. Menke, N. A. Ran, G. C. Bazan and R. H. Friend, *Joule*, 2018, **2**, 25–35.
57 X.-K. Chen and J.-L. Brédas, *Adv. Energy Mater.*, 2018, **8**, 1702227.

